AMERICAN ACADEMY OF OPHTHALMOLOGY®
In partnership with the AMERICAN GLAUCOMA SOCIETY

Glaucoma Rose Plot Analysis

Detecting Early Structural Progression Using Angular Histograms

Timothy E. Yap, MA, MRCP,[1,2] *Benjamin M. Davis, PhD,*[3,4] *Philip A. Bloom, FRCOphth,*[1,2] *M. Francesca Cordeiro, PhD, FRCOphth,*[1,2,4] *Eduardo M. Normando, MD, PhD*[1,2]

Purpose: To evaluate the novel Rose Plot Analysis (RPA) in the analysis and presentation of glaucoma structural progression data.

Design: Case-control image analysis study using retrospective retinal imaging series.

Subjects: Subjects with open-angle glaucoma with at least 5 registered spectral-domain OCT scans.

Methods: Glaucoma RPA was developed, combining a novel application of angular histograms and dynamic cluster analysis of circumpapillary retinal nerve fiber layer (cRNFL) OCT data. Rose Plot Analysis plots were created for each eye and each visit. Significant clusters of progression were indicated in red. Three masked clinicians categorized all RPA plots (progressing, not progressing), in addition to measuring the significant RPA area. A masked OCT series assessment with linear regression of averaged global and sectoral cRNFL thicknesses was conducted as the clinical imaging standard.

Main Outcome Measures: Interobserver agreement was compared between RPA and the clinical imaging standard. Discriminative ability was assessed using receiver-operating characteristic curves. The time to detection of progression was compared using a Kaplan–Meier survival analysis, and the agreement of RPA with the clinical imaging standard was calculated.

Results: Seven hundred fourty-three scans from 98 eyes were included. Interobserver agreement was significantly greater when categorizing RPA (κ, 0.86; 95% confidence interval [CI], 0.81–0.91) compared with OCT image series (κ, 0.66; 95% CI, 0.54–0.77). The discriminative power of RPA to differentiate between eyes that were progressing and not progressing (area under the curve [AUC], 0.97; 95% CI, 0.92–1.00) was greater than that of global cRNFL thickness (AUC, 0.71; 95% CI, 0.59–0.82; $P < 0.0001$) and equivalent to that of sectoral cRNFL regression (AUC, 0.97; 95% CI, 0.92–1.00). A Kaplan–Meier survival analysis showed that progression was detected 8.7 months sooner by RPA than by global cRNFL linear regression ($P < 0.0001$) in progressing eyes but was not sooner than with sectoral cRNFL ($P = 0.06$). Rose Plot Analysis showed substantial agreement with the presence of significant thinning on sectoral cRNFL linear regression (κ, 0.715; 95% CI, 0.578–0.853).

Conclusions: Rose Plot Analysis has been shown to provide accurate and intuitive, at-a-glance data analysis and presentation that improve interobserver agreement and may aid early diagnosis of glaucomatous disease progression. *Ophthalmology Glaucoma 2022;5:562-571 © 2022 by the American Academy of Ophthalmology. This is an open access article under the CC BY-NC-ND license (http://creativecommons.org/licenses/by-nc-nd/4.0/).*

Supplemental material available at www.ophthalmologyglaucoma.org.

Retinal nerve fiber layer (RNFL) thickness is commonly used as a structural biomarker in the investigation of patients with glaucoma. This parameter represents the health of the ganglion cell population from which the nerve fibers project. The speed and patient acceptability of OCT imaging has encouraged widespread, frequent use in disease monitoring, without harm to the patient. Thus, serial circumpapillary thickness measurements along a circular path around the optic nerve head complement functional outcomes (visual field testing) to inform clinicians on the stage, location, and rate of ganglion cell loss, aiding the diagnosis of glaucoma.

The thickness of the RNFL as measured by segmentation of cross-sectional OCT images has been shown to demonstrate reasonable discriminative and predictive abilities, often ahead of confirmed visual field loss.[1,2] However, the rate of disease progression is now routinely being used to individualize treatment in the context of existing glaucomatous damage, life expectancy, and comorbidities. The use of RNFL thinning to represent disease progression is evidenced by its association with worsening of visual field defects.[3,4] Therefore, it is paramount that structural biomarkers are developed, enabling early

https://doi.org/10.1016/j.ogla.2022.06.002
ISSN 2589-4196/22

detection of "preperimetric" disease progression and allowing timely instigation of therapy to prevent visual loss and blindness from end-stage disease.[5]

Progression analyses of circumpapillary RNFL (cRNFL) measures have been incorporated into the software of all major OCT platforms, with average rates of progression globally and sectorally assessed using linear regression over time. Although event-based analysis has been shown to possess equivalent accuracy,[6] trend-based methods are less susceptible to anomalous results and are useful for extrapolating future field loss in the context of patient age. In contrast to visual field testing, which can be limited by its subjective nature, a "learning effect,"[7] and poor reproducibility in the context of reduced visual acuity,[8] OCT technology lends itself well to determining the rate of progression through serial measures, with excellent repeatability in the majority of cases.[9] Variations in optic disc and RNFL morphology can limit the diagnostic power of single scans relative to a normative database, whereas a within-subject longitudinal assessment may be used to detect small amounts of structural change.[10]

With diagnostic technologies generating ever-increasing amounts of data, efficiently summarizing and communicating this information to facilitate clinical decision making requires the development of effective analysis and visualization methods. An appropriate analysis harnesses the power of the data to its fullest extent, whereas intuitive data visualization can better inform clinical decisions. Furthermore, the evolution of such clinical tools ensures adaptations are made to manage the increasing number of patients looked after worldwide.[11] We present the development of Rose Plot Analysis (RPA), a novel method of cRNFL OCT data analysis and presentation that is able to comprehensively summarize the rate and location of structural progression at a glance. The aim of this study was to investigate RPA's effect on the reproducibility of clinical decision making and its potential for improving early diagnosis, using both qualitative and quantitative assessments of RNFL thickness through time to represent the current clinical imaging standard of care.

Methods

RPA Development

Rose Plot Analysis was iteratively developed by a team of clinical ophthalmologists and scientific software developers. The unmet clinical need was described as at-a-glance data presentation to comprehensively summarize the progression statuses of glaucomatous eyes. Rose Plot Analysis displays a unique combination of information relating to an individual eye throughout the course of all visits, namely, the rate, location, and significance of RNFL thinning. These data are displayed in an angular histogram and, thus, are not summarized according to global or sectoral averages. The rate of thinning is represented by the height of the graph, the anatomic location of thinning is represented as the circumpapillary angular location on the angular histogram, and areas of thinning deemed to be significant are highlighted in red, according to the application of dynamic clustering (Fig 1).

Study Participants

This study was given ethical approval by the Health Regulatory Authority of the United Kingdom (IRAS 282562). The study was carried out in accordance with the Declaration of Helsinki. Fully anonymized data sets were used for the purposes of this study. Thus, no consent was deemed necessary. Consecutive, eligible eyes were enrolled by clinicians from glaucoma clinics at the Western Eye Hospital, Imperial College Healthcare National Health Service Trust, London, United Kingdom. Eligible eyes were diagnosed or under observation for open-angle glaucoma, had at least 5 referenced cRNFL scans, and had a minimum average global cRNFL of 50 μm (to avoid the floor effect[12]). Eyes were excluded if they had significant media opacity; if they had concomitant neurologic or ocular disease affecting the optic nerve, retinal health, or the eye's morphology; or if extremes of refractive error (±6 diopters spherical equivalent or ±3 diopters of astigmatism) were present.

Imaging Data

Images were acquired on a spectral-domain OCT imaging platform (Spectralis SD-OCT; Heidelberg Engineering). Built-in eye tracking and averaging processes were used to improve image quality. The built-in anatomic positioning system ensured accurate fovea-disc orientation throughout. Images were anatomically aligned between visits, and the RNFL layer was segmented automatically using the proprietary imaging software. Eyes were manually checked for imaging artifacts or segmentation errors and failure (including those caused by media opacity), and exclusions were made where present. No thresholding according to a quality indicator was conducted to avoid selection bias. Raw, numeric cRNFL data were extracted using a custom patch. This was comprised of 768 A-scans (point scans) from the 3.5-mm diameter circumpapillary circle, centered on the optic nerve head at each visit, in addition to global and sectoral averages (according to Garway-Heath sectors[13]). These data were imported into R (R Project for Statistical Computing[14]). Sectoral and global progression values were calculated using ordinary least squares linear regression through the time from baseline using R.[14]

The RPA protocol was as follows: for each patient visit, data were aligned and presented as coordinate polar plots before ordinary least squares linear regression was performed at each of the 768 retinal layer thickness measurements through time (days), normalized to a baseline (first) visit. As regions of progression were expected to be larger than individual A-scans, the resulting slopes were assessed for significant deviation from 0 using a 1-sample t test (assessment for regions of thinning only) before resulting P values were combined using a clustering × fast-search method, as previously described[15] (parameters, $\delta = 0.2$; $\rho = 2.0$). Assuming independence between resulting clusters, P values were pooled using the Fisher exact test,[16] and cluster progression was declared when α was $<1 \times 10^{-7}$ using the Holm–Bonferroni correction for multiple comparisons, with these regions presented in red. For the purpose of this study, data from each eye were evaluated independently.

Clinician OCT Grading (Clinical Imaging Standard)

To define the clinical imaging standard, OCT image series from study eyes were independently graded by 3 ophthalmologists (E.M.N., P.A.B., and T.E.Y.) masked from any additional clinical information. The images available to the graders included cRNFL profiles plotted against the manufacturer's default normative database, with the cRNFL thickness color coded into green (within normal limits, $P > 0.05$), amber (borderline, $P < 0.05$), and red

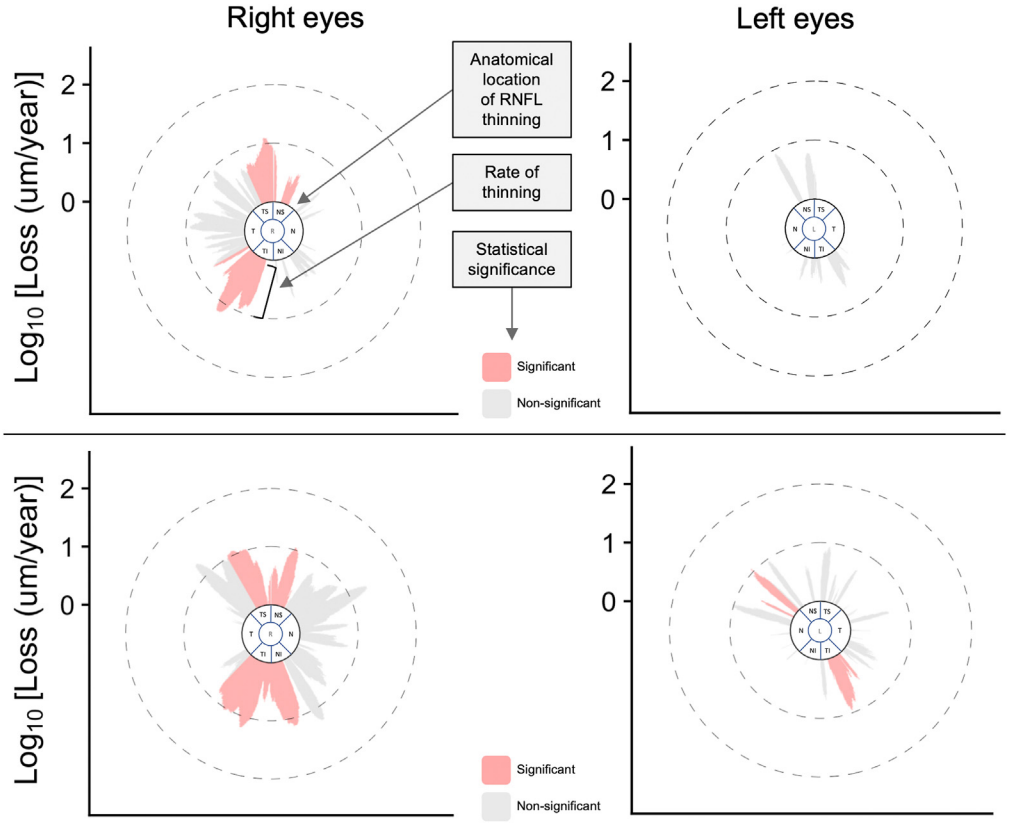

Figure 1. Examples of Rose Plot Analysis plots from 2 patients. Rose Plot Analysis uses the centripetal height of the graph to show the rate of thinning, the circumferential position to show the circumpapillary location of thinning, and the color of the graph to show statistical significance, in a single, at-a-glance plot. Top row: a patient with a significantly progressing right eye and stable left eye. Bottom row: a patient with a progressing right eye and a left eye with progression only highlighted using Rose Plot Analysis. Garway-Heath sectors are included centrally for anatomic orientation. Further examples are shown in Figure S1 (available at www.ophthalmologyglaucoma.org). L = left eye; N = nasal; NI = nasoinferior; NS = nasosuperior; R = right eye; RNFL = retinal nerve fiber layer; T = temporal; TI = temperoinferior; TS = temperosuperior.

(outside normal limits, $P < 0.01$) and 7 linear regression plots of averaged global and Garway-Heath sectoral cRNFL values through time, accompanied with the regression slope (μm/year) and statistical significance (P value). Eyes were graded by masked clinicians as progressing, stable, or unaffected, with the last 2 categories classed as not progressing. Progressing eyes were marked as progressing if they would be placed under enhanced monitoring or treatment would be initiated or upgraded. The majority consensus (progressing or not progressing) was used as the clinical imaging standard.

Quantitative OCT Grading

A quantitative assessment of OCT series was carried out using ordinary least squares linear regression of cRNFL thicknesses through time (days). This was performed for the averaged global cRNFL measurement and each of the 6 averaged Garway-Heath sector cRNFL values (temperosuperior, temporal, temperoinferior, nasoinferior, nasal, and nasosuperior) in the same manner as the proprietary progression analysis module. To simulate the progression analysis completed at each visit for each eye through time, the regression of averaged global and sectoral RNFL thicknesses was carried out between each visit and baseline, incorporating the data acquired in between. For continuous variable analysis, the regression slope was used. For binary analysis (progressing or not progressing), the presence of progression was defined as any series with statistically significant thinning ($P < 0.05$).

Clinician RPA Grading

All rose plots generated from RPA were graded independently by 3 ophthalmologists (E.M.N., P.A.B., and T.E.Y.) masked from any other imaging (including OCT scans) or further clinical information. Clinicians were asked to independently grade the plots as clinically progressing or not progressing after reviewing a standard operating procedure document explaining the concepts of RPA displays. Plots were presented to the clinicians and graded in a custom program designed in R. The majority binary decision of 3 clinicians was taken as the qualitative clinician RPA categorization.

Quantitative RPA Grading

Rose plots were quantitatively assessed by measuring the total area of red (statistically significant cluster progression) in each plot, thus removing subjectivity and interobserver variability. This continuous variable was calculated independently of the script used to generate the RPA plots and quantified the area of red (in pixels) seen by the clinicians in each plot. Each plot was analyzed using an ImageJ[17] macro to count red pixels.

Statistical Analysis

Targeted analyses using the qualitative and quantitative gradings of both RPA and OCT imaging were carried out, each to investigate particular aspects of the novel RPA methodology. These included interobserver agreement to investigate reliability, receiver-operator characteristic (ROC) curves to compare discriminative ability against objective measures, a time-to-event analysis to investigate the potential for early diagnosis, and 2-way tables to highlight agreement and safety (false-negative rates).

Interobserver agreement between the 3 masked clinicians (E.M.N., P.A.B., and T.E.Y.) for both RPA and OCT series was assessed using the Fleiss κ statistic. Agreement was regarded as none to slight when between 0.01 and 0.20, fair when 0.21 to 0.40, moderate when 0.41 to 0.60, substantial when 0.61 to 0.80, and almost perfect when 0.81 to 1.00.[18,19]

The ROC curves were used to compare the discriminative ability of an objective RPA assessment (quantitative RPA grading) with objective OCT parameters (quantitative OCT grading), namely, the global cRNFL linear regression slope and the global cRNFL thickness at the final visit. This was carried out using subjective and objective classifiers; the clinical imaging standard (clinician OCT categorization) and the presence of statistically significant sectoral cRNFL linear regression. The area under the ROC curve (AUROC) of 0.5 was interpreted as discrimination equivalent to chance, with an AUROC of 1 showing perfect discrimination. With a combination of parametric and nonparametric distributions of data, a parametric approach to ROC was maintained, as described previously.[20] The DeLong method was used to determine any significant differences between AUROCs.[21] Adjustment of P values for multiple comparisons used the conservative Bonferroni method.[22] A quantitative RPA assessment (red area) was correlated with linear regression of cRNFL values. The correlation was termed strong when the absolute value of r was > 0.7, moderate when r was > 0.5, and weak when r was > 0.3. All statistical analyses were carried out using R. The ROC curves were plotted using ROCit.[23]

Two-way tables were used to investigate the level of agreement of clinician RPA grading with the following 3 classifiers: the clinical imaging standard (clinician OCT grading) and the presence or absence of a statistically significant negative trend ($P < 0.05$) in the global cRNFL or any cRNFL sector using the percentage agreement and the Cohen κ statistic. A Kaplan–Meier survival analysis was used as a time-to-event analysis to simulate detection of progression through time in all eyes and just in those clinically labeled as progressing by the clinical imaging standard. The time to detection of progression was compared between clinician RPA grading and both the occurrence of a statistically significant linear trend ($P < 0.05$) in the global cRNFL and the presence of a statistically significant linear trend ($P < 0.05$) in any cRNFL sector. Statistical significance was declared when the P value was < 0.05 throughout.

Results

Study Population

There were 743 scans from 98 eyes that met the inclusion criteria for this study. The mean age of the patients (± standard deviation) was 68.2 ± 12.0 years; 47% of patients were men, and 53% were women; and 55% were right eyes, and 45% were left eyes. The mean starting visual field mean deviation was −4.0 ± 5.0 dB. The mean starting global average cRNFL was 79.1 ± 16.8 μm. The mean number of visits per eye was 7.6 ± 3.2 scans. These demographics and baseline statistics are separated into eyes classed as progressing and not progressing by the clinical imaging standard. There was a significantly thinner mean global cRNFL thickness in the progressing group ($P < 0.0001$). There was no significant difference in the starting mean deviation between the progressing and not-progressing groups ($P = 0.534$). There was also no significant difference between the number of visits in each image series between groups ($P = 0.058$; Table 1).

Interobserver Agreement

The 3-way agreement between the clinicians when categorizing OCT series to form the clinical imaging standard was 83% (κ, 0.66; 95% confidence interval [CI], 0.54–0.77). The 3-way agreement between the clinicians when categorizing RPA was significantly greater, at 90% (κ, 0.86; 95% CI, 0.81–0.91; Fig 2).

Discriminative Ability of RPA

The ability of RPA to discriminate between OCT series categorized as progressing and not progressing by the clinical imaging standard was an area under the curve (AUC) of 0.97 (95% CI, 0.92–1.00), which was significantly superior to that of the global cRNFL thickness (AUC, 0.71; 95% CI, 0.59–0.83; DeLong method $P < 0.0001$) and comparable to that of linear regression of the global cRNFL thickness (AUC, 0.97; 95% CI 0.92–1.00; $P = 1.00$; Fig 3).

The ability of RPA to discriminate between OCT series categorized as progressing and not progressing by the presence of any significant sectoral cRNFL thinning (AUC, 0.95; 95% CI, 0.90–0.99) was significantly superior to that of the global cRNFL thickness (AUC, 0.61; 95% CI, 0.50–0.73; $P < 0.0001$) and comparable to that of linear regression of the global cRNFL thickness (AUC, 0.94; 95% CI, 0.89–0.99; $P = 1.00$; Fig 3).

Agreement of RPA with the Clinical Imaging Standard

The agreement of clinician RPA categorization with the clinical imaging standard was 77.6% (κ, 0.555; 95% CI, 0.389–0.721). In all eyes where there was disagreement, RPA categorized the eyes as progressing, whereas the clinical imaging standard categorized them as not progressing (Fig S2, available at www.ophthalmologyglaucoma.org).

Agreement of RPA with Linear Regression of OCT Data

The agreement of the clinician RPA categorization with the presence of a statistically significant trend in global cRNFL thinning was 68.4% (κ, 0.38; 95% CI, 0.17–0.59). In all eyes where there was disagreement, RPA categorized the eyes as progressing, whereas the clinical imaging standard categorized them as not progressing (Fig S2, available at www.ophthalmologyglaucoma.org).

The agreement of the clinician RPA categorization with the presence of a statistically significant trend in sectoral cRNFL thinning was 85.7% (κ, 0.72; 95% CI, 0.58–0.85). In the eyes where there was disagreement, 11.2% of eyes were marked as progressing with RPA and 3% were marked as progressing with linear regression of sectoral cRNFL (Fig S2). Examples of RPA plots that were in agreement and disagreement with the clinical

Table 1. Baseline Characteristics of Eyes Included in the Study*

Patient Characteristics				
	Overall	*Progressing*	*Not Progressing*	P
Patients, n	91	25	66	-
Eyes, n	98	28	70	-
Mean age ± SD, years	67.8 ± 12.3	65.4 ± 11.6	68.7 ± 12.5	0.255
Gender, Male:Female %	47%:53%	52%:48%	45%:55%	0.396
Laterality (left eye:right eye)	55%:45%	48%:52%	57%:43%	0.257
Starting MD ± SD, dB	−4.0 ± 5.0	−4.5 ± 4.5	−3.8 ± 5.2	0.534
Starting global cRNFL thickness ± SD, μm	79.1 ± 16.8	74.3 ± 11.7	81.1 ± 18.2	<0.0001
Mean number of visits ± SD, n	7.5 ± 3.2	8.5 ± 3.8	7.1 ± 2.8	0.058

cRNFL = circumpapillary retinal nerve fiber layer; dB = decibels; MD = mean deviation; SD = standard deviation.
*The data have also been subdivided into those eyes categorized as progressing and not progressing by the clinical imaging standard (masked clinician assessment of OCT series).

imaging standard are displayed in Figure S1 (available at www.ophthalmologyglaucoma.org).

Correlation of RPA with Linear Regression

The RPA red areas were significantly different between those eyes graded as progressing and not progressing with the clinical imaging standard ($P < 0.0001$; n = 743). There was a strong, positive correlation between the RPA red area and the rate of global cRNFL thinning in eyes categorized as progressing by the clinical imaging standard ($r = 0.93$; $R^2 = 0.87$; $P < 0.0001$). To a much lesser extent, a weak correlation was present with the eyes labeled as not progressing by the clinical imaging standard ($r = 0.42$; $R^2 = 0.17$; $P < 0.001$). There was a strong, positive correlation between the RPA red area and the rate of sectoral cRNFL thinning (fastest progressing sector) both in eyes categorized as progressing ($r = 0.73$; $R^2 = 0.53$; $P < 0.0001$) and in eyes categorized as not progressing ($r = 0.74$; $R^2 = 0.55$; $P < 0.0001$) by the clinical imaging standard (Fig S2, available at www.ophthalmologyglaucoma.org).

Survival Analysis

A Kaplan–Meier survival analysis revealed statistically significant earlier detection of progression using clinician RPA categorization compared with the presence of significant thinning of global cRNFL using linear regression.

Among all patients at the end of year 1, 10% were marked as progressing with global cRNFL linear regression, and 41% were marked as progressing with RPA; at the end of year 2, 56% were marked as progressing with global cRNFL, and 78% were marked as progressing with RPA ($P < 0.0001$ overall). Median survival was > 912 days (95% CI, 883 to > 912 days) with global cRNFL and was 511 days (95% CI, 378–699 days) with RPA, with a reduction of at least 401 days ($P < 0.0001$). Exclusively among those eyes categorized as progressing by the clinical imaging standard, 21% were marked as progressing with global cRNFL and 71% were marked as progressing with RPA at the end of year 1, whereas 79% were marked as progressing with global cRNFL and 96% were marked as progressing with RPA at the end of year 2. Median survival was 527 days (95% CI, 456–598 days) with

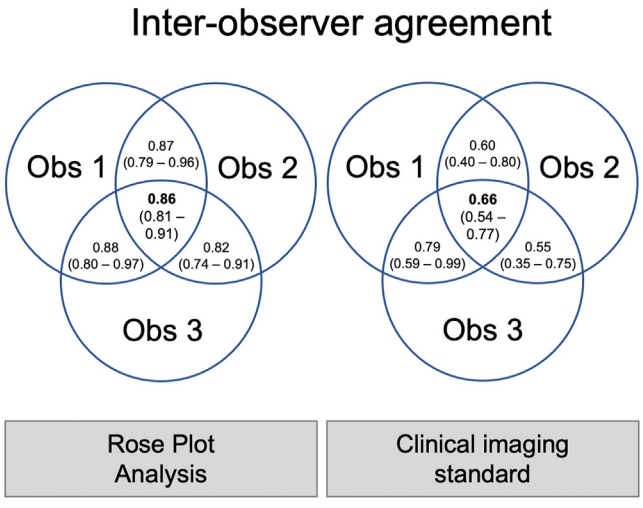

Figure 2. Comparison of masked clinician interobserver agreement assessing Rose Plot Analysis and OCT series (clinical imaging standard). Rose Plot Analysis demonstrated significantly greater agreement (Fleiss κ, 0.86 [95% confidence interval, 0.81–0.91] vs. 0.66 [95% confidence interval, 0.54–0.77], respectively) than OCT when assessed for disease progression. Obs = observer.

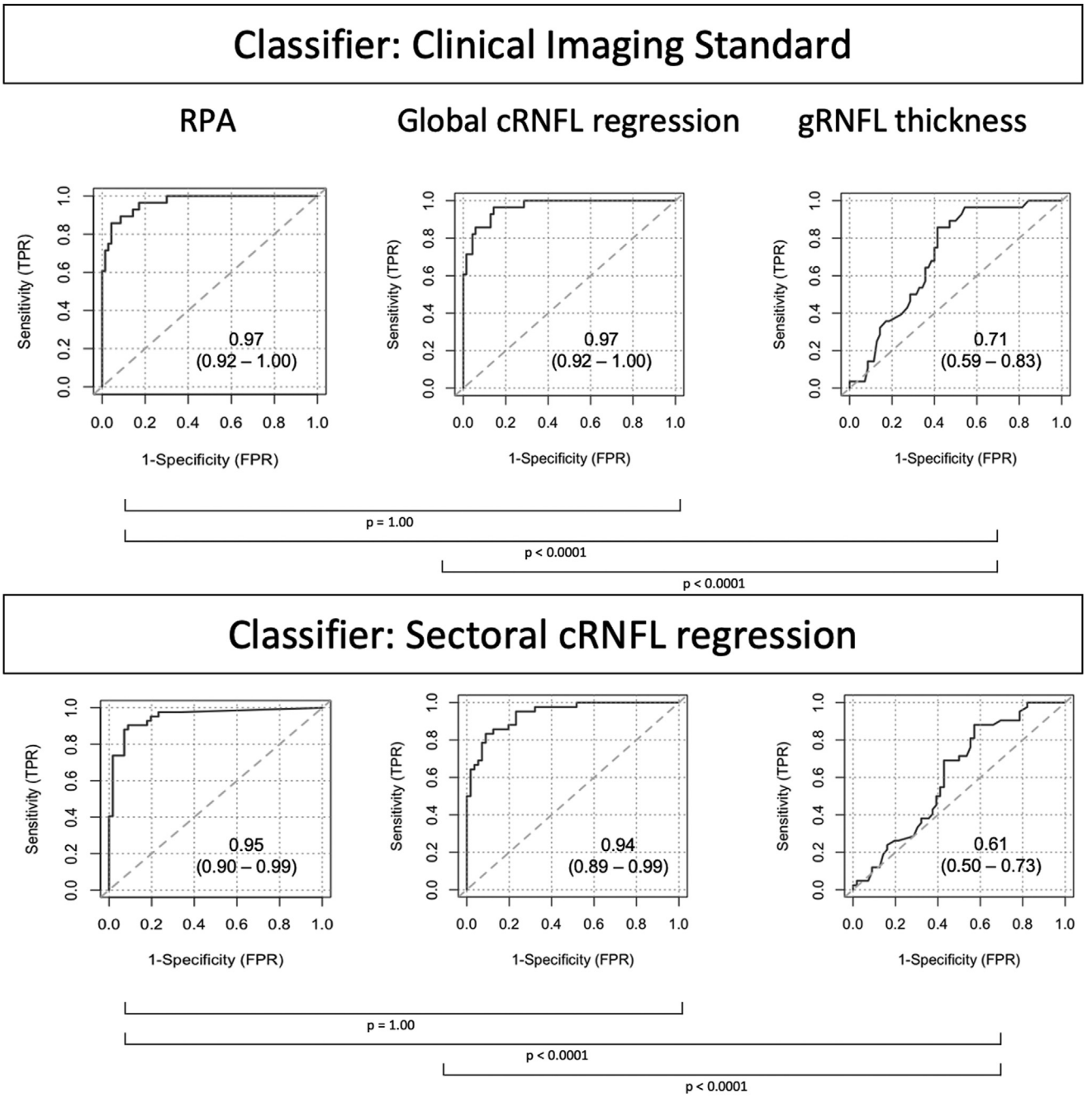

Figure 3. Receiver-operating characteristic curves showing the ability of RPA (red area), the rate of global cRNFL thinning, and the mean global cRNFL thickness (latest) to discriminate between eyes with disease that is progressing and not progressing. The area under the receiver-operator characteristic (95% confidence interval) is shown for each plot. Eyes were classified as progressing and not progressing by 2 methods. Upper row: clinician assessment of OCT series (clinical imaging standard). Bottom row: the presence of at least 1 circumpapillary sector demonstrating significant thinning using linear regression. A significant difference was found between the area under the receiver-operator characteristics of mean gRNFL thickness and both RPA and gRNFL regression in the case of both classifiers (DeLong method, adjusted P value < 0.0001). cRNFL = circumpapillary retinal nerve fiber layer; gRNFL = global cRNFL; RPA = Rose Plot Analysis.

global cRNFL and 263 days (95% CI, 182−365 days) with RPA, with a reduction of 264 days ($P < 0.0001$; Fig 4).

Among all patients at the end of year 1, 32% were marked as progressing with sectoral cRNFL linear regression (any sector) compared with 41% marked as progressing with RPA; at the end of year 2, 73% were marked as progressing with sectoral cRNFL compared with 78% marked as progressing with RPA. Median survival was 699 days (95% CI, 502−875 days) with sectoral cRNFL and 511 days (95% CI, 378−699 days) with RPA ($P = 0.064$). Among patients categorized as progressing by the

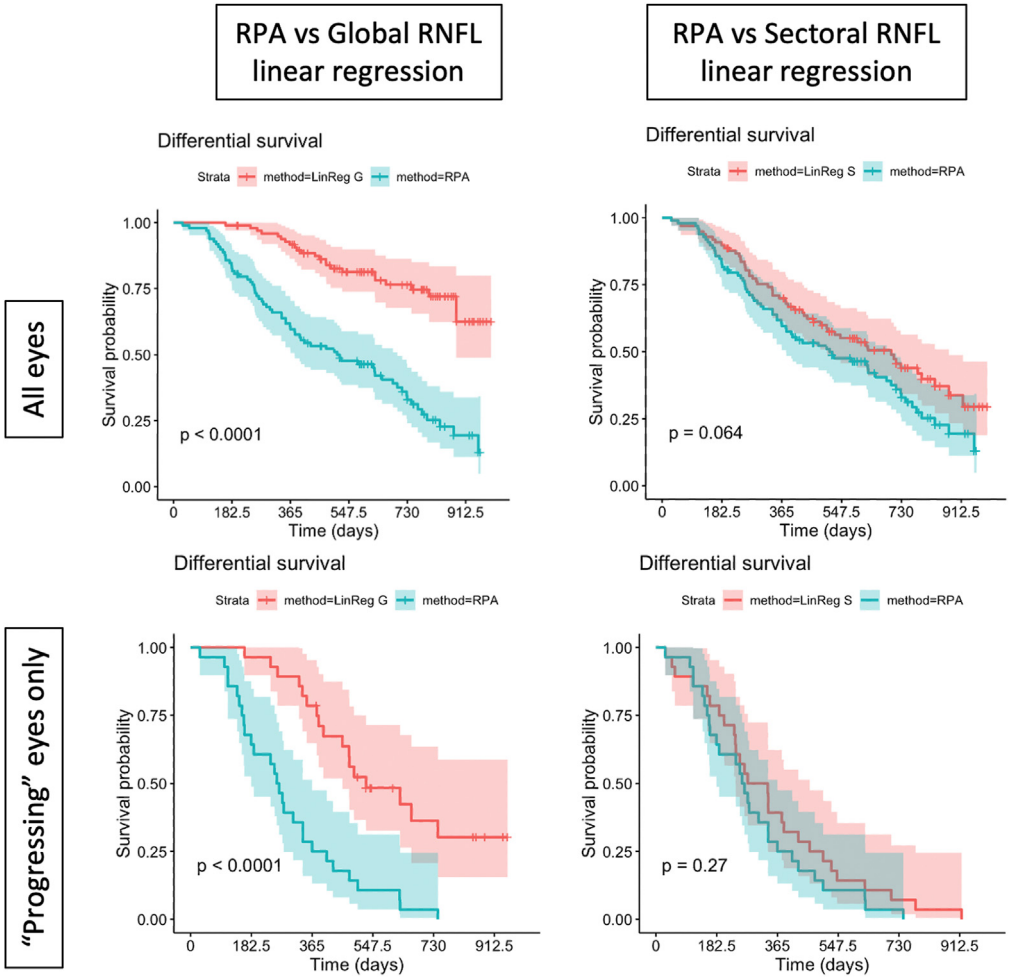

Figure 4. Kaplan–Meier survival curves comparing the detection of progression using RPA (green) and linear regression (red) in the same eyes with time (1 event = detection of progression). The majority of clinician assessment of RPA was compared against 2 other markers: the presence of global and sectoral circumpapillary RNFL (cRNFL) statistically significant thinning on linear regression. This was examined in 2 cohorts: all study eyes (top row) and those graded as progressing by the clinical imaging standard (bottom row). Statistically significant improvements were seen with RPA versus the global cRNFL thinning in both cohorts (median survival, all eyes: LinReg G, >912.5 days [95% confidence interval [CI], 883 to >912.5 days] and RPA, 511 days [95% CI, 378–699 days; $P < 0.0001$]; progressing eyes only: LinReg G, 527 days [95% CI, 456–598 days] and RPA, 263 days [95% CI, 182–365 days; $P < 0.0001$]) but not compared with sectoral cRNFL thinning (median survival, all eyes: LinReg S, 699 days [95% CI, 502–875 days] and RPA, 511 days [95% CI, 378–699; $P = 0.064$]; progressing eyes only: LinReg S, 306 days [95% CI, 239–462 days] and RPA, 262 days [95% CI, 182–365; $P = 0.270$]). LinReg G = linear regression of the global circumpapillary retinal nerve fiber layer; LinReg S = linear regression of the sectoral circumpapillary retinal nerve fiber layer; RNFL = retinal nerve fiber layer; RPA = Rose Plot Analysis.

clinical imaging standard, at the end year 1, 61% were marked as progressing with sectoral cRNFL compared with 71% marked as progressing with RPA, and at the end of year 2, 93% were marked as progressing with sectoral cRNFL compared with 96% marked as progressing with RPA. Median survival was 306 days (95% CI, 239–462 days) with sectoral cRNFL and 262 days (95% CI, 182–365 days) with RPA ($P = 0.270$; Fig 4).

Discussion

This study has demonstrated RPA as a novel analysis and visualization tool that is able to accurately and intuitively display comprehensive structural progression data. Incorporated in the output are the rate, location, and significance of RNFL thinning, creating a powerful, at-a-glance plot that is anatomically orientated and easily interpretable. This study has demonstrated that RPA can improve agreement between clinicians and potentially assist in the early diagnosis of glaucoma progression.

The imperfect agreement between clinical end points when detecting glaucoma progression has previously been demonstrated.[24] Furthermore, poor interobserver agreement plagues the reproducibility of clinical decisions and equality in standards of care.[25–27] When assessing optic disc photographs and standard automated perimetry, interrater κ values have been quoted as 0.16 and 0.13, respectively.[26] Although OCT has been shown to accurately and

consistently detect preexisting glaucomatous damage,[26] refinement of a progression analysis is required to differentiate those with progressive disease requiring more aggressive treatment. The use of an objective progression analysis to aid assessment of changes between visits has been demonstrated in visual field testing.[28] However, the OCT equivalent using linear regression confined to predefined circumpapillary sectors is time consuming to review and increases the potential for interobserver variability. Consequently, the lack of an agreed systematic approach results in clinicians giving varying degrees of importance to biomarkers when assessing patients. Hood[29] suggested a single-page display of OCT data to guide systematic assessments for structural damage, also aiding correlations to functional data. In a similar manner, our study demonstrates that RPA can act as a decision-making tool for progression analysis. The improved interobserver agreement promises great potential to provide better consistency and standardization of treatment decisions, with RPA displaying circumferential progression data in a single, circular plot. Furthermore, owing to the ease with which the results can be anatomically correlated, the plot is a compelling, qualitative and quantitative, novel assessment tool.

The widespread uptake of structural imaging is believed to have increased diagnostic sensitivity for glaucoma, with many OCT studies differentiating glaucomatous from healthy eyes. A recent meta-analysis[1] reported a pooled AUROC of 0.897 (95% CI, 0.887−0.906) for cRNFL measures. However, stratifying eyes in such a way does not confer the rate of progression, whereas the clinical objective is often to highlight those in most need of urgent treatment. Thus, plotting a dynamic process, as with RPA, has more important implications on the future trajectory of the patient's visual status and the immediate need for treatment. In the evolution of visual field progression analyses, event-based and trend-based approaches have been compared, with the results demonstrating similar performances between the 2 methods.[30] Similar comparisons of progression analysis methodology have been made for OCT imaging, with some superiority of the trend-based approach adopted in RPA[31] reported. In further developing trend-based approaches, pointwise linear regression in visual field testing increased the resolution of analyses in comparison to regression of summary measures[32,33]; in analogous fashion, pointwise linear regression of circumpapillary thickness points has been built into RPA, with the aim of identifying earlier structural changes.

The use of angular histograms in glaucoma progression is a novel application in the field of medical imaging. However, the plots have been successfully applied in other fields, namely, meteorology.[34] The unique ability to plot vectors in a circumferential manner conveys both magnitude and spatial information for applications such as wind speed and direction, where both may be critically important. In the case of glaucoma, it is characteristically the supertemporal and inferotemporal nerve fiber bundles that seem particularly vulnerable to damage and, thus, may be differentiated from other patterns of nerve fiber loss.[29]

In contrast to the averaged circumpapillary sectors commonly used in clinical practice,[13] the variable sector size of RPA allows intelligent, multidimensional rose formation while giving more statistical weight to clusters of progressing circumpapillary points. Not only does this function as effective noise filtration, but it also is likely to allow for a greater range of developing RNFL defect sizes to be highlighted.[35] For instance, small, discrete bundles of nerve fibers can often display subtle thinning in early disease[36] that may not be of sufficient size to influence summary values based on sectoral or global averages. The multidimensional intelligence of RPA displays has the potential for yet further expansion by incorporating multiple circle scan diameters in transparent rose plots to emphasize thinning at multiple circumpapillary diameters. Thus, the improved granularity of RPA is in keeping with better diagnostic sensitivity, avoiding the pitfalls of diagnosing "red" and "green" disease statuses when summary measures are taken at face value.[37] This theory is matched by the results of this study, demonstrating significantly a reduced time to detect progression using RPA compared with the global RNFL linear regression (and near significance with the sectoral indices). The excellent results in terms of sensitivity (very few cases where RPA did not detect progression labeled by other methods) when compared with regression indices mean that RPA is a safe tool in reassuring clinicians of the absence of progression, potentially helping overburdened services.[38]

Limitations of this study include the exclusion of functional outcomes while instead comparing with a clinical imaging standard that is used as structural information as part of the patient assessment. The exact relationship between structure and function assessed with the biomarkers available is complex and continues to be fully characterized[39,40]; therefore, the challenge in glaucoma research remains finding a gold standard allowing full adherence to the recommended Standards for Reporting of Diagnostic Accuracy Studies guidelines[41,42] for diagnostic accuracy studies. It is critical that studies of any new assessment of the clinical utility of a new diagnostic technique follow such guidelines; our study was not designed in this way. To link the earliest changes observed on RPA with functional loss, longitudinal, prospective studies with regular visual field monitoring would be required. Within this, recruitment could be stratified by baseline disease severity to ascertain the effect on RPA sensitivity as the minimum cRNFL floor thickness is approached[12] and, conversely, to exclusively examine "preperimetric" patients, where RPA has the greatest potential to improve early diagnoses. Prior work associating points of visual field loss with circumpapillary structural locations[29] may then be used to incorporate existing functional losses on the rose plots or even predict vulnerable points on the visual field.[40]

The future of structural biomarkers in glaucoma may lie in developing discerning combinations of multimodal imaging specifically tailored to the clinical task at hand for clinicians appropriately qualified to interpret the data in the

context of the entire patient. Increasing attention is being given to glaucoma as a retinal disease, with posterior pole scanning protocols providing glaucoma diagnosis with an AUROC of 0.885 (95% CI, 0.869−0.901) for the macular ganglion cell complex, along with mapping of structural changes to functional losses in other novel methods of data presentation.[43] Trend-based progression analyses using these data are still to be refined. However, to utilize historic cRNFL data, RPA is well placed to "signpost" attention to particular regions of interest that can be extrapolated to examination findings and other investigations, in keeping with topographic, structure-functional relationships.[44] With our results demonstrating the multifaceted potential that RPA has in clinical glaucoma care, we propose its clinical introduction as a structural representative incorporated into the comprehensive patient assessment to improve clinical decision making and the care of our patients.

Footnotes and Disclosures

Originally received: February 11, 2022.
Final revision: May 26, 2022.
Accepted: June 1, 2022.
Available online: June 15, 2022. Manuscript no. OGLA-D-22-00026R2.

[1] Western Eye Hospital, Imperial College Healthcare NHS Trust (ICHNT), London, United Kingdom.
[2] Imperial College Ophthalmic Research Group (ICORG), Imperial College London, United Kingdom.
[3] Central Laser Facility, Rutherford Appleton Laboratory, Oxfordshire, United Kingdom.
[4] Glaucoma and Retinal Neurodegeneration Group, Department of Visual Neuroscience, UCL Institute of Ophthalmology, London, United Kingdom.

Presented as a poster at ARVO Denver, May 1−4, 2022, Denver, Colorado.

Disclosures:
All authors have completed and submitted the ICMJE disclosures form.

The author(s) have made the following disclosure(s): M.F.C.: Speaker's fees and contribution in kind−Heidelberg Engineering.

The other authors have no proprietary or commercial interest in any materials discussed in this article.

HUMAN SUBJECTS: Human subjects were included in this study. This study was given ethical approval by the Health Regulatory Authority of the United Kingdom (IRAS 282562). The study was carried out in accordance with the Declaration of Helsinki. Fully anonymized data sets were used for the purposes of this study. Thus, no consent was deemed necessary.

No animal subjects were included in this study.

Author Contributions:

Conception and design: Yap, Davis, Bloom, Cordeiro, Normando

Data collection: Yap

Analysis and interpretation: Yap, Davis, Normando

Obtained funding: N/A; Study was performed as part of the authors' regular employment duties. No additional funding was provided.

Overall responsibility: Yap, Davis, Bloom, Cordeiro, Normando

Abbreviations and Acronyms:
AUC = area under the curve; **AUROC** = area under the receiver-operator characteristic; **CI** = confidence interval; **cRNFL** = circumpapillary retinal nerve fiber layer; **RNFL** = retinal nerve fiber layer; **ROC** = receiver-operator characteristic; **RPA** = Rose Plot Analysis.

Keywords:
Glaucoma, Progression analysis, Retinal nerve fiber layer, Rose plot, OCT.

Correspondence:
Eduardo M. Normando, MD, PhD, Western Eye Hospital, Imperial College Healthcare NHS Trust (ICHNT), 153-173 Marylebone Rd, Marylebone, London NW1 5QH, United Kingdom. E-mail: e.normando@nhs.net.

References

1. Kansal V, Armstrong JJ, Pintwala R, Hutnik C. Optical coherence tomography for glaucoma diagnosis: an evidence based meta-analysis. *PLoS One*. 2018;13:e0190621.
2. Lalezary M, Medeiros FA, Weinreb RN, et al. Baseline optical coherence tomography predicts the development of glaucomatous change in glaucoma suspects. *Am J Ophthalmol*. 2006;142:576−582.
3. Miki A, Medeiros FA, Weinreb RN, et al. Rates of retinal nerve fiber layer thinning in glaucoma suspect eyes. *Ophthalmology*. 2014;121:1350−1358.
4. Tatham AJ, Medeiros FA. Detecting structural progression in glaucoma with optical coherence tomography. *Ophthalmology*. 2017;124:S57−S65.
5. Susanna Jr R, De Moraes CG, Cioffi GA, Ritch R. Why do people (still) go blind from glaucoma? *Transl Vis Sci Technol*. 2015;4:1.
6. Yu M, Lin C, Weinreb RN, et al. Risk of visual field progression in glaucoma patients with progressive retinal nerve fiber layer thinning: a 5-year prospective study. *Ophthalmology*. 2016;123:1201−1210.
7. Chauhan BC, Garway-Heath DF, Goñi FJ, et al. Practical recommendations for measuring rates of visual field change in glaucoma. *Br J Ophthalmol*. 2008;92:569−573.
8. Matsuura M, Hirasawa K, Murata H, Asaoka R. The relationship between visual acuity and the reproducibility of visual field measurements in glaucoma patients. *Invest Ophthalmol Vis Sci*. 2015;56:5630−5635.
9. Töteberg-Harms M, Sturm V, Knecht PB, et al. Repeatability of nerve fiber layer thickness measurements in patients with glaucoma and without glaucoma using spectral-domain and time-domain OCT. *Graefes Arch Clin Exp Ophthalmol*. 2012;250:279−287.
10. Zhang X, Dastiridou A, Francis BA, et al. Comparison of glaucoma progression detection by optical coherence tomography and visual field. *Am J Ophthalmol*. 2017;184:63−74.
11. Tham YC, Li X, Wong TY, et al. Global prevalence of glaucoma and projections of glaucoma burden through 2040: a systematic review and meta-analysis. *Ophthalmology*. 2014;121:2081−2090.
12. Bowd C, Zangwill LM, Weinreb RN, et al. Estimating optical coherence tomography structural measurement floors to

improve detection of progression in advanced glaucoma. *Am J Ophthalmol*. 2017;175:37–44.
13. Garway-Heath DF, Poinoosawmy D, Fitzke FW, Hitchings RA. Mapping the visual field to the optic disc in normal tension glaucoma eyes. *Ophthalmology*. 2000;107:1809–1815.
14. RStudio Team. *RStudio: Integrated Development for R*. Boston, MA: R, Inc.; 2015.
15. Rodriguez A, Laio A. Machine learning. Clustering by fast search and find of density peaks. *Science*. 2014;344:1492–1496.
16. Owen AB. Karl Pearson's meta-analysis revisited. *Ann Statist*. 2009;37:3867–3892.
17. Schneider CA, Rasband WS, Eliceiri KW. NIH Image to ImageJ: 25 years of image analysis. *Nat Methods*. 2012;9:671–675.
18. Cohen J. A coefficient of agreement for nominal scales. *Educ Psychol Meas*. 1960;20:37–46.
19. McHugh ML. Interrater reliability: the kappa statistic. *Biochem Med (Zagreb)*. 2012;22:276–282.
20. Hajian-Tilaki KO, Hanley JA, Joseph L, Collet JP. A comparison of parametric and nonparametric approaches to ROC analysis of quantitative diagnostic tests. *Med Decis Making*. 1997;17:94–102.
21. DeLong ER, DeLong DM, Clarke-Pearson DL. Comparing the areas under two or more correlated receiver operating characteristic curves: a nonparametric approach. *Biometrics*. 1988;44:837–845.
22. Dunn OJ. Multiple comparisons among means. *J Am Stat Assoc*. 1961;56:52–64.
23. Khan MRA, Brandenburger T. ROCit. https://CRAN.R-project.org/package=ROCit. Accessed May 16, 2020.
24. Banegas SA, Antón A, Morilla-Grasa A, et al. Agreement among spectral-domain optical coherence tomography, standard automated perimetry, and stereophotography in the detection of glaucoma progression. *Invest Ophthalmol Vis Sci*. 2015;56:1253–1260.
25. Moreno-Montañés J, Antón V, Antón A, et al. Intraobserver and interobserver agreement of structural and functional software programs for measuring glaucoma progression. *JAMA Ophthalmol*. 2017;135:313–319.
26. Blumberg DM, De Moraes CG, Liebmann JM, et al. Technology and the glaucoma suspect. *Invest Ophthalmol Vis Sci*. 2016;57. OCT80–OCT85.
27. Viswanathan AC, Crabb DP, McNaught AI, et al. Interobserver agreement on visual field progression in glaucoma: a comparison of methods. *Br J Ophthalmol*. 2003;87:726–730.
28. Nouri-Mahdavi K, Hoffman D, Ralli M, Caprioli J. Comparison of methods to predict visual field progression in glaucoma. *Arch Ophthalmol*. 2007;125:1176–1181.
29. Hood DC. Improving our understanding, and detection, of glaucomatous damage: an approach based upon optical coherence tomography (OCT). *Prog Retin Eye Res*. 2017;57:46–75.
30. Wu Z, Medeiros FA. Comparison of visual field point-wise event-based and global trend-based analysis for detecting glaucomatous progression. *Transl Vis Sci Technol*. 2018;7:20.
31. Leung CK-S, Lin C, Yu M. Trend-based progression analysis (TPA): a new algorithm for visualizing the topology of progressive retinal nerve fiber layer (RNFL) thinning in glaucoma. *Invest Ophthalmol Vis Sci*. 2015;56, 3980–3980.
32. Fitzke FW, Hitchings RA, Poinoosawmy D, et al. Analysis of visual field progression in glaucoma. *Br J Ophthalmol*. 1996;80:40–48.
33. O'Leary N, Chauhan BC, Artes PH. Visual field progression in glaucoma: estimating the overall significance of deterioration with permutation analyses of pointwise linear regression (PoPLR). *Invest Ophthalmol Vis Sci*. 2012;53:6776–6784.
34. Droppo JG, Napier BA. Wind direction bias in generating wind roses and conducting sector-based air dispersion modeling. *J Air Waste Manag Assoc*. 2008;58:913–918.
35. Leung CK, Mohamed S, Leung KS, et al. Retinal nerve fiber layer measurements in myopia: an optical coherence tomography study. *Invest Ophthalmol Vis Sci*. 2006;47:5171–5176.
36. Jonas JB, Schiro D. Localised wedge shaped defects of the retinal nerve fibre layer in glaucoma. *Br J Ophthalmol*. 1994;78:285–290.
37. Chong GT, Lee RK. Glaucoma versus red disease: imaging and glaucoma diagnosis. *Curr Opin Ophthalmol*. 2012;23:79–88.
38. Morley AM, Murdoch I. The future of glaucoma clinics. *Br J Ophthalmol*. 2006;90:640–645.
39. Zhu H, Crabb DP, Fredette MJ, et al. Quantifying discordance between structure and function measurements in the clinical assessment of glaucoma. *Arch Ophthalmol*. 2011;129:1167–1174.
40. Kihara Y, Montesano G, Chen A, et al. Policy-driven, multimodal deep learning for predicting visual fields from the optic disc and OCT imaging. *Ophthalmology*. 2022 Feb 21;S0161-6420(22),00156-7. https://doi.org/10.1016/j.ophtha.2022.02.017. Online ahead of print.
41. Cohen JF, Korevaar DA, Altman DG, et al. STARD 2015 guidelines for reporting diagnostic accuracy studies: explanation and elaboration. *BMJ Open*. 2016;6:e012799.
42. Fidalgo BM, Crabb DP, Lawrenson JG. Methodology and reporting of diagnostic accuracy studies of automated perimetry in glaucoma: evaluation using a standardised approach. *Ophthalmic Physiol Opt*. 2015;35:315–323.
43. Hood DC, Raza AS, De Moraes CG, et al. Evaluation of a one-page report to aid in detecting glaucomatous damage. *Transl Vis Sci Technol*. 2014;3:8.
44. Ferreras A, Pablo LE, Garway-Heath DF, et al. Mapping standard automated perimetry to the peripapillary retinal nerve fiber layer in glaucoma. *Invest Ophthalmol Vis Sci*. 2008;49:3018–3025.